RESEARCH REPORT

Mechanical properties of $Al_{88}(Y_{1-x}Ce_x)_2Ni_9Fe_1$ (x=0, 0.5, 1) amorphous alloys containing nanoscale fcc-Al particles

Yeong-Hwan KIM*, Akihisa INOUE** and Tsuyoshi MASUMOTO**

Amorphous $Al_{88}(Y_{1-x}Ce_x)_2Ni_9Fe_1$ alloys containing nanoscale fcc-Al particles have been found to exhibit tensile fracture strength (σ_f) and hardness (HV) higher than those of amorphous single phase alloys with the same compositions, without detriment to good bending ductility. The particle size of the fcc-Al phase increases in the range of 3 to 30 nm with a decrease in cooling rate. The HV and Young's modulus (E) increase monotonously with increasing volume fraction of the fcc phase (V_f), while the σ_f shows a maximum in the V_f range of 5 to 26% (e.g., 1560 MPa at 25% V_f for $Al_{88}Ce_2Ni_9Fe_1$). The increase in σ_f in the V_f range below 26% is presumably due to an enhancement of the resistance to shear deformation caused by the nanoscale fcc particles which have hardness higher than that for the amorphous phase with the same compositions. The highest σ_f for the $Al_{88}Ce_2Ni_9Fe_1$ alloy is much higher than that (1320 MPa) for the $Al_{88}Y_2Ni_9Fe_1$ alloy. It is presumably a reason for this difference that the bonding force between Al and Ce atoms is stronger than that between Al and Y.

Keywords: ultrahigh strength, aluminum base alloy, amorphous phase, nanoscale fcc particle, rapid solidification

(*Received October* 11, 1991)

1. Introduction

The development of light-metal base alloys with mechanical properties superior to conventional duralumin alloys has strongly been desired for the last decade because of an increasing demand for transport capacity, especially in an aerospace field. It has recently been found[1),2)] that high tensile strengths exceeding 980 MPa and good bending ductility are obtained for Al-Ln-Ni (Ln=rare-earth metal) amorphous alloys. However, there are some disadvantages that the Al-Ln-Ni amorphous alloys contain expensive and reactive rare-earth metals above 5 at% and become brittle upon annealing-induced crystallization. Accoringly, we have carried out a systematic study on the determination of an optimum alloy compcsition to overcome these disadvantages. More recently, we have found[3)] that the Al-Y-Ni amorphous allloys with low solute concentrations containing nanoscale fcc-Al particles exhibit further improved tensile strengths as compared with those for the amorphous single phase alloys with the same composition, without detriment to bending ductility. Subsequently, it has been reported[4),5)] that the enhanced tensile strength caused by the dispersion of the nanoscale fcc-Al particles reaches as high as 1470 MPa for $Al_{88}Y_2Ni_8Mn_2$. However, little has been known about the effect of the replacement of rare-earth metal by other transition metals on the microstructure and mechanical properties for Al-Ln-Ni-Fe amorphous alloys containing finely dispersed fcc-Al particles. The aim of this paper is to examine the microstructure, thermal stability and mechanical properties for $Al_{88}(Y_{1-x}Ce_x)_2Ni_9Fe_1$ alloys consisting of coexistent amorphous and fcc-Al phases and to investigate the reason for the achievement of the ultrahigh tensile strengths.

2. Experimental Procedure

Quaternary alloy ingots with compositions $Al_{88}(Y_{1-x}Ce_x)_2Ni_9Fe_1$ (x=0, 0.5, 1) were prepared by arc melting mixtures of pure Al, Ni, Fe and Y or Ce metals in a purified argon atmosphere. Rapidly solidified ribbons with a width of 1.6 mm and different thicknesses ranging from 15 to 30

* Graduate School, Department of Materials Science, Tohoku University (Sendai-shi, Miyagi).
** Institute for Materials Research, Tohoku University (Sendai-shi, Miyagi).

μm were prepared by a single roller melt-spinning technique. The volume fraction of fcc-Al phase (V_f) was controlled by changing either the rotation speed of copper roller with a diameter of 200 mm in the range of 20 to 83 s^{-1} (1200 to 5000 rpm) or the ejecting temperature of molten alloy. Rapidly solidified structure was examined by X-ray diffractometry and transmission electron microscopy (TEM). The TEM samples were prepared by thinning electrolytically the melt-spun ribbons in a solution of 25% nitric acid and 75% methanol at 243 K. The tensile fracture morphology was examined by scanning electron microscopy (SEM). Crystallization temperature (T_x) and heat of crystallization (ΔH_x) were measured by differential scanning calorimetry (DSC) at a heating rate of 0.67 K/s. The V_f in the melt-spun ribbons was determined from the ratio of the amount of heat released during heating from room temperature to 850 K to the heat of crystallization in an amorphous single phase[6]. Hardness and tensile strength were examined by a Vickers microhardness tester with 0.49 N (50 gf) load and an Instron-type tensile testing machine at a strain rate of 8.3×10^{-4} s^{-1}, respectively.

3. Results

3.1 Microstructure

Fig. 1 shows the bright-field electron micrographs and electron diffraction patterns of $Al_{88}Y_1Ce_1Ni_9Fe_1$ ribbons produced at different rotation speeds of roller. As the rotation speed (cooling rate) decreases from 50 to 20 s^{-1}, the structure changes from amorphous to amorphous plus crystalline phases. The electron diffraction patterns reveal that the crystalline phase has an fcc structure with a lattice parameter (a_0) of 0.405 nm. The a_0 value is nearly equal to that of pure Al metal (0.4047 nm)[7] and hence the fcc phase is regarded as an Al-rich phase. Although the particle size increases with a decrease of cooling rate, it is in the range of 3 to 10 nm. The particle size is concluded to be considerably smaller than the previously reported value (3 to 30 nm)[4),5] for the $Al_{88}Y_2Ni_9Fe_1$ alloy.

In order to confirm the particle size and homogeneous distribution of the fcc-Al phase in the rapidly solidified $Al_{88}Y_1Ce_1Ni_9Fe_1$ alloy with V_f of 26% shown in Fig. 1(c), the dark-field electron micrograph taken from a part of the $(111)_{Al}$ and $(200)_{Al}$ reflection rings is shown in **Fig. 2**. The fcc particles with an average size of 5 nm disperse homogeneously and isolatedly, in agreement with the results obtained from Fig. 1. The homogeneous dispersion of the nanoscale fcc-Al particles has also been confirmed for the $Al_{88}Y_2Ni_9Fe_1$ alloy by high-resolution electron microscopy[5].

3.2 Thermal stability

Fig. 3 shows the DSC curves of the melt-spun $Al_{88}Ce_2Ni_9Fe_1$ ribbons having the amorphous or the mixed structure, along with the data of V_f. Two exothermic peak are seen in each temperature range of 457 to 510 and 593 to 643 K. It is confirmed from the X-ray diffractometry that the two exothermic peaks are due to the precipitation of fcc-Al phase from the amorphous phase and the transformation of the remaining amorphous matrix to Al plus compound phases, respectively. The magnitude of the first exothermic peak due to the precipitation of Al phase gradually decreases with decreasing rotation speed of roller, while that of the second exothermic peak remains almost unchanged, indicating that the volume fraction of the fcc-Al phase in the melt-spun ribbons increases with a decrease of cooling rate. It is thus said that the precipitation amount of the Al phase can be controlled by changing rotation speed of the roller. In ad-

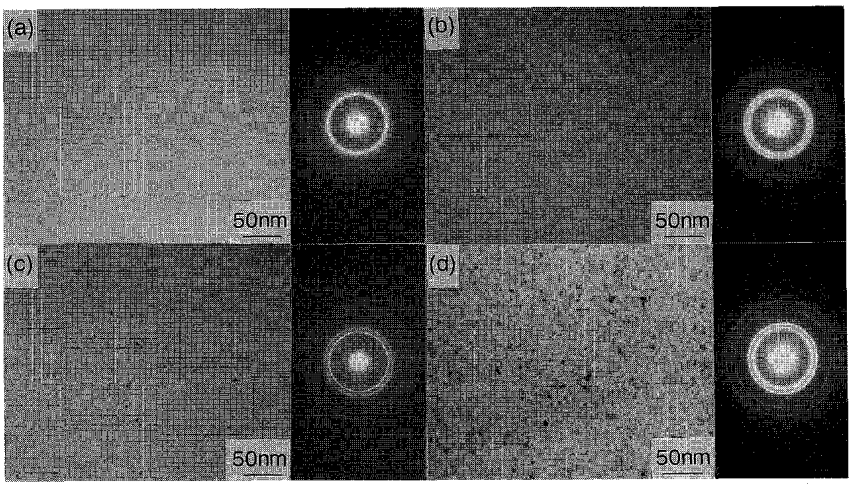

Fig. 1 Changes in the bright-field electron micrograph and electron diffraction pattern of a rapidly solidified $Al_{88}Y_1Ce_1Ni_9Fe_1$ alloy with rotation speed of roller: (a) 50 s^{-1}, (b) 33 s^{-1}, (c) 25 s^{-1}, (d) 20 s^{-1}.

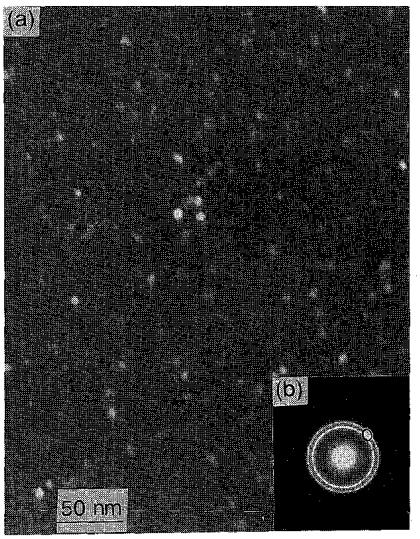

Fig. 2 Dark-field electron micrograph (a) and electron diffraction pattern (b) of $Al_{88}Y_1Ce_1Ni_9Fe_1$ with $V_f=26\%$. The circle in the diffraction pattern represents the position and size of the aperture.

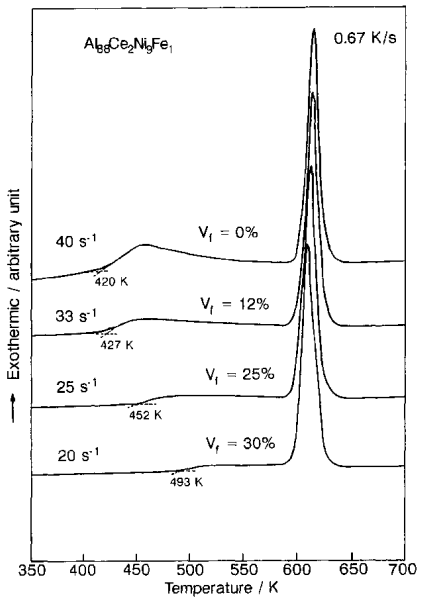

Fig. 3 Differential scanning calorimetric curves of rapidly solidified $Al_{88}Ce_2Ni_9Fe_1$ ribbons with an amorphous single phase or coexistent amorphous and fcc-Al phases.

dition, the onset temperature (T_x) of precipitation of the fcc-Al phase tends to increase with increasing V_f, indicating an enhancement of thermal stability of the remaining amorphous phase. T_x of the $Al_{88}Ce_2Ni_9Fe_1$ amorphous

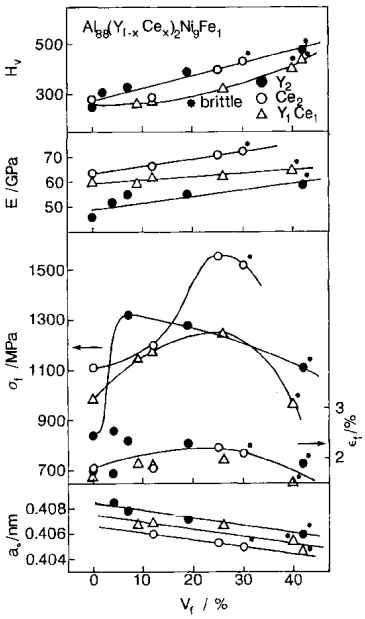

Fig. 4 Vickers Hardness (HV), Young's modulus (E), tensile fracture strength (σ_f), fracture elongation (ε_f) and lattice parameter (a_0) as a function of volume fraction of Al phase (V_f) for rapidly solidified $Al_{88}(Y_{1-x}Ce_x)_2Ni_9Fe_1$ alloys.

alloy is about 45 K higher than that[4),5)] of the $Al_{88}Y_2Ni_9Fe_1$ amorphous alloy, indicating the significant enhancement of thermal stability by the replacement of Y by Ce. A similar change in the DSC curve has also been observed[4),5)] for the $Al_{88}Y_2Ni_9Fe_1$ and $Al_{88}Y_1Ce_1Ni_9Fe_1$ alloys with the same mixed structure.

3.3 Mechanical properties

All the Al-rich amorphous ribbons containing nanoscale fcc-Al particles below $V_f\simeq30\%$ exhibited good bending ductility and its deformation structure was similar to the common feature for ductile melt-spun amorphous alloys.

The relacement effect of rare-earth metals (Ln) on the mechanical properties was examined for $Al_{88}(Y_{1-x}Ce_x)_2Ni_9Fe_1$ ($x=0$, 0.5, 1) alloys consisting of amorphous and nanoscale fcc particles. As shown in **Fig. 4**, Vickers Hardness (HV) and Young's modulus (E) increase monotonously with an increase of V_f for the three alloys, presumably because the strength is higher for the fcc-Al phase than for the amorphous phase. The HV value is nearly the same for $Al_{88}Y_2Ni_9Fe_1$ and $Al_{88}Ce_2Ni_9Fe_1$ and tends to be slightly lower for $Al_{88}Y_1Ce_1Ni_9Fe_1$. On the other hand, σ_f and fracture elongation (ε_f) show maximum values in the V_f range of 5 to 26% and decrease with a further increase of V_f, because of an enhancement of embrittlement tendency, as described later. The maximum σ_f ($\sigma_{f,max}$)

value increases significantly to 1560 MPa for $Al_{88}Ce_2Ni_9Fe_1$ without Y element and shows the lowest value of 1250 MPa for $Al_{88}Y_1Ce_1Ni_9Fe_1$, in agreement with the tendency for HV. Furthermore, the optimum V_f value at which the highest σ_f values are obtained increases with the replacement of Y by Ce. These compositional effects seem to result from the changes in hardness and particle size of the fcc-Al phase embedded in the amorphous matrix with the replacement of Y by Ce. As shown in Figs. 1 and 2 and Refs. 4) and 5), the particle size of the fcc-Al phase in the three $Al_{88}(Y_{1-x}Ce_x)_2Ni_9Fe_1$ alloys in which the $\sigma_{f,max}$ is obtained is nearly constant (about 4-7 nm). It is therefore said that the V_f value at which the fcc-Al particle with the constant size of about 5 nm is obtained tends to increase with the replacement of Y by Ce and the enhancement of $\sigma_{f,max}$ for the $Al_{88}Ce_2Ni_9Fe_1$ alloy is due mainly to the increase of the optimum V_f value at which the particle size of about 5 nm is obtained. On the other hand, the lattice parameter (a_0) decreases monotonously with an increase of V_f and slightly with the replacement of Y by Ce. The a_0 values in the V_f range below about 30% are larger than that of pure Al (0.4047 nm) and hence the fcc-Al phase is a solution saturated with Ni, Fe and Y or Ce.

Thus, the $\sigma_{f,max}$ reaches as high as 1560 MPa for the $Al_{88}Ce_2Ni_9Fe_1$ amorphous alloy containing nanoscale fcc-Al particles. It is notable that the strength value is about 3 times higher than that for the conventional superduralumin (Al-Cu-Mg-Mn alloy). The achievement of the ultrahigh $\sigma_{f,max}$ in the mixed phase alloys is very important in the subsequent development of a high-strength bulk material with light weight, because of an additioal advantage that the optimum mixed structure is obtained at a cooling rate lower than that for the formation of an amorphous single phase.

Fig. 5 shows tensile fracture surface appearance for the melt-spun $Al_{88}Y_1Ce_1Ni_9Fe_1$ ribbons with an amorphous single phase or the mixed structure. As shown in Fig. 5(a) and (b), a significant fraction in the fracture surface area for the mixed phase alloy with V_f of 9% is occupied by the smooth region which occurred by the shear deformation experienced prior to failure. This indicates that the uniform dispersion of nanoscale fcc-Al particles in the amorphous matrix does not cause a detrimental influence on the ease of shear deformation. Although the feature in the fracture process at V_f=9% is similar to that for an amorphous single phase alloy with good ductility, one can notice a remarkably different fracture behavior. That is, the fracture surface for the majority of the mixed phase ribbons with V_f of 26% consists of elongated and tangled vein pattern as shown in Fig. 5(c). This difference suggests that the nanoscale fcc-Al particles with a particle size smaller than the size of the deformation region ($\simeq$10 to 20 nm)[8] in the shear sliding act as

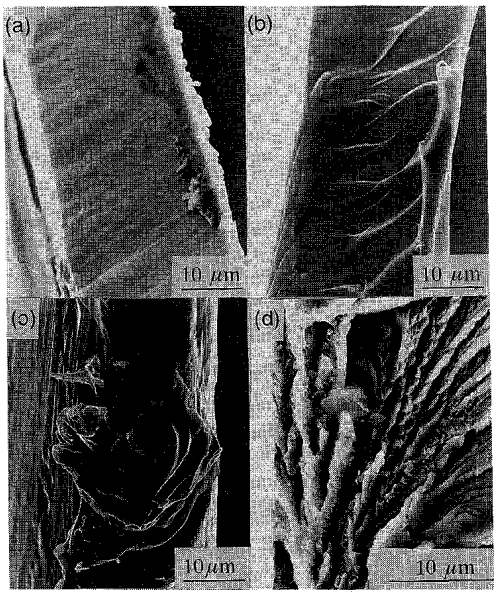

Fig. 5 Scanning electron micrographs showing the tensile fracture appearance of rapidly solidified $Al_{88}Y_1Ce_1Ni_9Fe_1$ ribbons with different V_f values. (a) 0%, (b) 9%, (c) 26%, (d) 40%.

an effective resistance to shear deformation and enhance the degree of local adiabatic heating, leading to a more significant viscous flow of the amorphous matrix, particularly at an optimum V_f. The increase of V_f to 30% results in the change into the fracture morphology characterized by the coexistence of shell-like region as shown in Fig. 5(d), in addition to the vein and smooth regions, indicating an enhancement of the degree of embrittlement. This result indicates that, when fcc-Al particles above an optimum amount are included, the existence of the fine fcc-Al particles causes a decrease of ductility. It is pointed out from these results that the homogeneous precipitation of the nanoscale fcc-Al particles brings about a significant change in fracture morphology and the change is particularly remarkable at an optimum V_f.

4. Discussion

As the mechanism for the increase in mechanical strenghts for the mixed phase alloys, we have previously reported[3)~5)] that the homogeneous dispersion and nanoscale size of the fcc-Al particles are dominant factors for the achievement of the high mechanical strengths in the melt-spun Al-Y-Ni ternary and Al-Y-Ni-M (M=Mn, Fe or Co) quaternary alloys, in addition to the high hardness of fcc-Al particle itself. It is shown in Fig. 1 and Fig. 2 that the microstructure in rapidly solidified $Al_{88}(Y_{1-x}Ce_x)_2Ni_9Fe_1$ alloys consists of nanoscale fcc-Al particles

homogeneously dispersed in their amophous matrix. A similar strengthening mechanism based on the homogeneous dispersion of the nanoscale fcc-Al particles can be applied for the interpretation of the increase in mechanical strengths for the present mixed phase alloys.

The reason for the achievement of the ultrahigh mechanical strengths is investigated in terms of some parameters such as the refinement effect of grain size, the mixing rule and the bonding nature among constituent atoms which have generally been thought to have a significant effect on the mechanical strengths. As shown in section 3, the fcc-Al phase is a supersaturated solution containing Ni, Fe and Y or Ce elements which are more than the equilibrium solubility limit. Furthermore, it has previously been reported[3)~5)] that the mechanical strength of the fcc-Al phase itself is higher than that of the amorphous single phase. The HV of the $Al_{88}(Y_{1-x}Ce_x)_2Ni_9M_1$ alloys with the mixed structure increases continuously with an increase of V_f. However, the σ_f shows a maximum at V_f=5-26% and decreases with a further increase of V_f because of the increase in the embrittlement tendency. It is thus said that the change in σ_f with V_f for the highly ductile alloys in the V_f range below about 26% is explained by the mixing rule between the amorphous and fcc-Al phases. The satisfaction of the mixing rule in the increase of σ_f only for the ductile alloys in the nanoscale dispersion state seems to be related to the unique deformation and fracture behaviors of the mixed phase alloys. That is, the majority of the fracture surface of the mixed phase ribbon with an optimum V_f, at which the $\sigma_{f,max}$ is obtained, consists of elongated and tangled vein pattern, indicating that the rupture occurred mainly through the viscous flow mechanism. There are some data[3)~5)] that the hardness of the fcc-Al phase is higher than that of amorphous phase with the same composition. Accordingly, when the particle size and interparticle spacing of the fcc-Al particle are comparable to and/or smaller than that of the local deformation band ($\simeq$10 to 20 nm)[8)] in shear sliding and the precipitation amount of fcc-Al particles is optimum, the fcc-Al particles can act as an effective resistance to shear deformation. As a result, the degree of local adiabatic heating is enhanced, leading to a more significant viscous flow of the amorphous matrix. Thus, the suppression of the shear slip caused by the dispersion hardening prior to final fracture is concluded to result in the increase of σ_f.

It is shown in Fig. 4 that the HV and E values increase monotonously with increasing V_f. This result indicates clearly that the nanoscale fcc-Al phase has the strength higher than that of the amorphous matrix. Here, we estimate the tensile fracture strength (σ_F) of the nanoscale fcc-Al particle in the coexisting amorphous and fcc-Al phases by using the conventional mixing rule; $\sigma_m=\sigma_A(1-V_f)+\sigma_F V_f$, where σ_m, σ_A and σ_F are tensile strengths of the mixed phase alloy, the amorphous single phase and the fcc-Al particle, respectively. Since the σ_m of the $Al_{88}Ce_2Ni_9Fe_1$ alloy with V_f=25% is 1560 MPa and the σ_A is 1100 MPa, the resulting σ_F is 2940 MPa which corresponds to 42% of the theoretical value ($\sigma\simeq E/10=7000$ MPa)[9)]. The estimated σ_F value is about 4 times as high as the previously reported highest σ_f value (700 MPa)[10)] for the fcc-Al solid solution. The marked difference is thought to be closely related to the nanoscale size of the fcc-Al particles. As reported previously in Ref. 5, no internal defects are observed in the nanoscale fcc particles, presumably because the annihilation of internal defects along the boundary between amorphous and fcc phases causes a decrease in internal energy of the nanoscale fcc particle. The absence of internal defects seems to bring about a marked increase in mechanical strength, as compared with those for the conventional crystalline structure containing a high density of internal defects, through a similar mechanism which has been recognized[11)] for whiskers with perfect crystalline structure.

Finally, the reason for the compositional dependence of the mechanical strengths in the $Al_{88}(Y_{1-x}Ce_x)_2Ni_9M_1$ alloys with the mixed structure is discussed on the basis of the V_f and the strength of the amorphous matrix itself. As shown in section 3, the $\sigma_{f,max}$ for the mixed $Al_{88}(Y_{1-x}Ce_x)_2Ni_9Fe_1$ alloys is mainly dominated by V_f because the particle size at which the $\sigma_{f,max}$ is obtained is nearly constant. In addition, the compositional effect of σ_f is also thought to be contributed to strength of the amorphous matrix[3),5)]. Accordingly, it is necessary that the bonding force among the constituent atoms in the amorphous phase is taken into consideration, in addition to the V_f value. It has been clarified by anomalous X-ray scattering[12)], electronic property[13)] and enthalpy relaxation[14)] that the atomic pairs between Al and Y or Ce atoms develop preferentially in Al-Y-Ni and Al-Ce-Ni amorphous alloys. Consequently, the replacement effect of Y by Ce on σ_f of the present alloys with constant Al, Ni and Fe contents seems to be explained by the difference in the bonding force between Al and Y or Ce atoms. As shown in Fig. 4, the σ_f of the amorphous single phase $Al_{88}Y_2Ni_9Fe_1$ alloy is smaller than that for the $Al_{88}Ce_2Ni_9Fe_1$ alloy. This result indicates that the difference in the bonding force between Al and Y or Ce atoms must be also taken into consideration in the explanation of the compositional dependence of $\sigma_{f,max}$ for these mixed alloys, in addition to the contribution of V_f and particle size. Furthermore, the HV and σ_f values show minima for the $Al_{88}Y_1Ce_1Ni_9Fe_1$ alloy. Considering that the equilibrium phase diagram in Y and Ce system[15)] is in an immisible type in a solid state, it is inferred that the simultaneous existence of

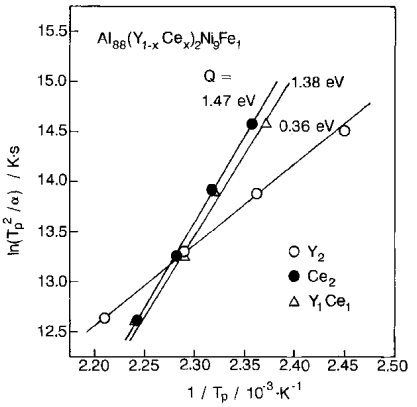

Fig. 6 Kissinger plots of $\ln(T_p^2/\alpha)$ against $1/T_p$ for rapidly solidified $Al_{88}(Y_{1-x}Ce_x)_2Ni_9Fe_1$ amorphous alloys. The α and T_p represent the scanning rate and the temperature of exothermic peak due to the precipitation of fcc-Al phase.

the elements with the repulsive bonding force causes a detrimental influence[16] to the mechanical strength. It is therefore concluded that the replacement effect on the $\sigma_{f,max}$ in the $Al_{88}(Y_{1-x}Ce_x)_2Ni_9Fe_1$ alloys appears through the combination of the V_f and particle size of the fcc-Al phases and the magnitude of the bonding force among the constituent atoms in the amorphous matrix.

Subsequently, the increase in the optimum V_f leading to $\sigma_{f,max}$ with the replacement of Y by Ce for the mixed $Al_{88}(Y_{1-x}Ce_x)_2Ni_9Fe_1$ alloys is discussed in terms of the particle size refinement of the fcc-Al phase. As shown in Figs. 1, 2 and 4, the $\sigma_{f,max}$ is obtained for the mixed phases with a nearly constant particle size of about 5 nm. The deviation of the particle size from the optimum size results in the decrease in σ_f. **Fig. 6** shows that the activation energy for precipitation of the fcc-Al phase (Q) in the $Al_{88}(Y_{1-x}Ce_x)_2Ni_9Fe_1$ amorphous allloys evaluated by the Kissinger method[17] increases significantly from 0.36 eV to 1.47 eV with the replacement of Y by Ce. Consequently, the nucleation and growth of fcc-Al particles are concluded to be retarded with the replacement of Y by Ce. The retardation causes an increase in the V_f value where the optimum particle size ($\simeq$5 nm) of the fcc-Al phase is obtained, resulting in the tendency that the $\sigma_{f,max}$ is obtained in the higher V_f range. The significant increase in the Q value is presumably because the melting temperature of an $Al_{11}Ce_3$ equilibrium compound is 100 K higher than that of Al_3Y compound[15] and hence the interaction of Al-Ce pairs is considerably stronger than that of Al-Y pair. Alternatively, considering that the interparticle distance is roughly proportional to the particle size, the V_f required to obtain an optimum particle size increases with the replacement of Y by Ce.

5. Summary

In order to obtain ultrahigh mechanical strengths in Al-Ln-Ni-Fe (Ln=lanthanide metal) alloys consisting of coexistent amorphous and fcc-phases and to clarify the mechanism for the ultrahigh mechanical strength, the microstructure and mechanical properties of melt-spun $Al_{88}(Y_{1-x}Ce_x)_2Ni_9Fe_1$ (x=0, 0.5, 1) alloys were examined. The results obtained are summarized as follows.

(1) The structure of the three alloys consists of coexistent amorphous and fcc-Al phase and the volume fraction of the fcc-Al phase (V_f) increases with a decrease of cooling rate (with a decrease of roller speed). The fcc-Al phase has nanoscale particle sizes which increase from 3 to 30 nm with an increase of V_f.

(2) The HV and E increase with an increase of V_f, because the hardness of the fcc supersaturated solution is higher than that of the amorphous phase with the same composition. However, the σ_f and ε_f in the $Al_{88}(Y_{1-x}Ce_x)_2Ni_9Fe_1$ alloys show maxima at V_f=5-26%. The combined characteristics of good ductility and ultrahigh σ_f above 1300 MPa are obtained in the wide V_f range from 5 to 35% for the Al-Y-Ni-Fe alloys and the σ_f value is about 40% higher than that of the amorphous single phase alloys with the same compositions. The highest $\sigma_{f,max}$ reaches 1560 MPa for the $Al_{88}Ce_2Ni_9Fe_1$ alloy. The increase in σ_f value is presumably due to the increase of the resistance to shear slip caused by homogeneous dispersion of the nanoscale fcc-Al particles.

(3) The increase in optimum V_f value leading to the highest σ_f with the replacement of Y by Ce is due to the retardation of nucleation and growth of the fcc-Al phase to achieve an optimum particle size ($\simeq$5 nm) in the $Al_{88}(Y_{1-x}Ce_x)_2Ni_9Fe_1$ alloys. The increase of the $\sigma_{f,max}$ with the replacement of Y by Ce in the mixed $Al_{88}(Y_{1-x}Ce_x)_2Ni_9M_1$ alloys is presumably because of the stronger bonding force for Al-Ce pair than for Al-Y pair as well as the larger V_f value leading to an optimum fcc-Al particle size for the Al-Ce-Ni-Fe alloy.

Acknowledgement

One of the authors (A. Inoue) gratefully acknowledes support for this research by a grant from the Light Metal Educational Foundation, Inc.

References

1) A. Inoue, K. Ohtera, A.P. Tsai and T. Masumoto: Jpn. J. Appl., Phys., **27** (1988), L479.
2) A. Inoue, K. Ohtera and T. Masumoto: Sci. Rep. Res. Inst. Tohoku Univ., A-**35**, No.1 (1990), 115.
3) Y.H. Kim, A. Inoue and T. Masumoto: Mater. Trans., JIM, **32** (1991), 331.

4) Y.H. Kim, A. Inoue and T. Masumoto: Mater. Trans., JIM, **31** (1990), 747.
5) Y.H. Kim, A. Inoue and T. Masumoto: Mater. Trans., JIM, **32** (1991), 599.
6) A. Inoue, H. Tomioka and T. Masumoto: J. Mater. Sci., **18**, (1983), 153.
7) Powder Diffraction File, Inorganic Phases, 4-0787 (ICDA Pub., S. Weissmann ed., Swarthmore, 1989).
8) T. Masumoto and R. Maddin: Acta Met., **19** (1971), 725.
9) A. Kelly, W.R. Tyson and A.H. Cottrel: Phil. Mag., **15** (1967), 567.
10) A. Inoue, H. Yamaguchi, M. Kikuchi and T. Masumoto: Sci. Rep. Res. Inst. Tohoku Univ., **A-35** (1990), 101.
11) R.L. Mehan and J.A. Herzog: Whisker Technology, ed. A.P. Levitt, Wiley-Interscience, New York, (1970), 157.
12) E. Matsubara, Y. Waseda, A. Inoue, K. Ohtera and T. Masumoto: Z. Naturforsch, **44a** (1989), 814.
13) M. Pont, J. Gonzalo, K.V. Rao and A. Inoue: Phys. Rev. B, **40** (1989), 1345.
14) Y.H. Kim, A. Inoue and T. Masumoto: J. Non-Cryst. Solids, **127** (1991), 233.
15) Binary Alloy Phase Diagram (2nd ed.), ed. T.B. Massalski, ASM Int'l., Ohio, (1990), pp. 135, 237, 1130.
16) A. Inoue, K. Ohtera, K. Kita and T. Masumoto: Jpn. J. Appl. Phys., **27** (1988), L1796.
17) H.E. Kissinger: Anal. Chem., **29** (1957), 1702.